The Journal of Clinical Pharmacology
2021, 61(4) 506–514

DOI: 10.1002/jcph.1762

Unusual Distribution Kinetics of Gadoxetate in Healthy Human Subjects Genotyped for OATP1B1: Application of Population Analysis and a Minimal Physiological-Based Pharmacokinetic Model

Michael Weiss, PhD[1] and Werner Siegmund, MD[2]

Abstract

Gadoxetate (Gd-EOB-DTPA) is a hepatobiliary-specific contrast agent for magnetic resonance imaging. Using a minimal physiological-based pharmacokinetic (PBPK) model, it has been shown for the first time, that the rapid initial decline of plasma concentration after intravenous injection is the result of an uptake into hepatocytes rather than of a distribution into the extravascular extracellular space. About 50% of the steady-state distribution volume is related to hepatic uptake. The hepatic extraction ratio and hepatic clearance estimated based on the liver model as a part of the PBPK model were in accordance with literature data. The same holds for the predicted time course of the amount of gadoxetate in liver parenchyma. In elucidating the impact of OATP1B1 genotype (*1a/*1a and *15/*15) on the pharmacokinetics of gadoxetate, we found that tissue uptake and back-transfer rates were significantly reduced, whereas the hepatic sinusoidal efflux rate was significantly increased in carriers of the *15/*15 haplotype compared with those of the *1a/*1a (wild type). The model is potentially useful for determining hepatic kinetic parameters and distribution properties of drugs.

Keywords

distribution clearance, hepatic transporters, gadoxetate, pharmacokinetic modeling, tissue uptake

The analysis of distribution kinetics of drugs in the body has received little attention in the past. This is mainly because the intercompartmental clearance of mammillary compartment models does not provide useful information on the distribution process of drugs in the body because these compartments have no physiological or anatomical meaning. Consequently, they are not suitable for comparison of distribution properties of different drugs. Here, we applied the measure "total distribution clearance,"[1,2] that is, independent of a specific pharmacokinetic model, to characterize the distribution kinetics of liver cell-specific gadolinium-ethoxybenzyl-dietylenetriamine-pentaacetic acid (Gd-EOB-DTPA), gadoxetate, used in contrast-enhancing magnetic resonance imaging (MRI).[3] Gadoxetate (plasma protein binding, 10%; molecular weight, 72 572; N-butanol/water partition coefficient, logP = −2.11) is transported into hepatocytes by the organic anion transporting polypeptide (OATP) 1B1, OATP1B3, and back-flux into the sinusoids via the transport protein MRP3 and/or bidirectional-acting OATPs.[3] The secretion into bile is mediated by MRP2.[4] Because the efflux from hepatocytes is slower than the uptake, gadoxetate accumulates in the liver. Gadoxetate does not distribute into red cells and is not metabolized and not reabsorbed from the gut after biliary excretion. Renal excretion contributes about 50% to total clearance. In a recent study it was shown that genetic polymorphisms of OATP1B1 significantly influences the hepatic uptake of gadoxetate in healthy human subjects using gadoxetate-enhanced MRI.[5] The whole-body distribution kinetics of gadoxetate is somewhat unclear. It was assumed to distribute quickly throughout the extracellular extravascular space.[6–8] It has been stated that because

[1]Department of Pharmacology, Martin Luther University Halle-Wittenberg, Halle, Germany
[2]Department of Clinical Pharmacology, Center of Drug Absorption and Transport (C_DAT), University Medicine, Greifswald, Germany

Submitted for publication 4 September 2020; accepted 22 September 2020.

Corresponding Author:
Michael Weiss, PhD, Department of Pharmacology, Martin Luther University, Halle-Wittenberg, Halle 06097, Germany
Email: michael.weiss@medizin.uni-halle.de

of early hepatocyte uptake, an interstitial phase would be absent.[9,10]

In this article, we first report the reanalysis of the plasma concentration-time data from this study using a 3-compartment model. We found that the whole-body distribution of gadoxetate was in contrast with the assumption of a rapid transfer into the extravascular, extracellular space, which is characteristic for the distribution kinetics of extracellular markers. Second, to explain this result, the plasma concentration-time data were also analyzed using a minimal physiological-based pharmacokinetic (PBPK) model. This enabled us to clarify whether hepatic uptake plays a major role in the whole-body distribution kinetics of gadoxetate and to provide information on its hepatic disposition to predict the time course of hepatic enhancement. Finally, evaluation of plasma concentration-time data from healthy carriers of the wild-type and a loss-of-function protein of the selective hepatic uptake transporter OATP1B1 offered new insight into the distribution and elimination kinetics of gadoxetate in human liver.

Methods

Data

The data were obtained from a previous pharmacokinetic/pharmacogenomic study in healthy subjects who also underwent gadoxetate-enhanced MRI. Pharmacokinetics and hepatic enhancement of gadoxetate were evaluated after intravenous administration of 25 μmol/kg gadoxetate (0.1 mL/kg of body weight; Primovist; Bayer Healthcare, Berlin, Germany).[5] The reevaluation has been in line with the written informed consent of the previous study, which had been approved by the Independent Ethics Committee of the University Medicine of Greifswald and had been registered by EudraCT (2006-005249-13) and ClinicalTrials.gov (NCT01420211). The plasma concentration-time data in subjects of the *SLCO1B1**1a/*1a haplotype (n = 12, wild type) and those of the *SLCO1B1**15/*15 (n = 9, loss-of-function variant) were reanalyzed with both a mammillary 3-compartment model and a minimal PBPK model. In the PBPK model, renal clearance as estimated using cumulative urinary excretion of gadoxetate was used in the analysis.

Data Analysis

The concentration-time data of gadoxetate after intravenous bolus injection were analyzed by a population approach with maximum likelihood estimation (MLEM) via the expectation-maximization algorithm implemented in ADAPT 5 software.[11] One major advantage of the population analysis is that interindividual and intraindividual variability can be quantified by simultaneous fitting of the data across subjects. Thus, the MLEM program provides estimates of the population mean and intersubject variability as well as of the individual subject parameters (conditional means). We assumed log-normally distributed model parameters and that the standard deviation of the measurement error is a linear function of the measured quantity. "Goodness of fit" was assessed using the Akaike information criterion (AIC) and by plotting the predicted-versus-measured responses. S-Plus was used for statistical analysis.

Mammillary Compartment Model

The best fit was obtained with a 3-compartment model. The distribution clearance (CL_D, formerly called CL_M) as a model-independent measure of the whole-body distribution kinetics was calculated as described previously[1]:

$$CL_D = \frac{1}{\left(\frac{V_1}{V_{ss}}\right)^2 \frac{1}{CL_{01}} + \left(\frac{V_2}{V_{ss}}\right)^2 \frac{1}{CL_{02}}} \quad (1)$$

where V_0 denotes the volume of the central compartment and V_1 and V_2 are volumes of the peripheral compartments; CL_{01} and CL_{02} are the respective distribution clearances; and $V_{ss} = V_0 + V_1 + V_2$ is the steady-state distribution volume. Note that CL_D is a purely phenomenological parameter determined by the area under the mixing, or equilibrium, distribution curve (AUC_D) in a hypothetical noneliminating system (CL = 0), that is, the area between C_D (t) and the concentration reached at equilibrium, $C_D(\infty) = C_{D,ss} = D_{iv}/V_{ss}$[12]:

$$CL_D = \frac{D_{iv}}{AUC_D} \quad (2)$$

Physiologically Based Pharmacokinetic Model

The structure of the minimal model for gadoxetate disposition is shown in Figure 1. The differential equations are provided in Supplementary Materials. A similar model was previously used to analyze the disposition kinetics of rocuronium[13] and insulin[14] in humans. The adjustable model parameters k_{tp} (tissue-to-plasma transport constant), PS (permeability-surface area product), k_{in} (uptake into hepatocytes), k_{out} (sinusoidal back-flux), and k_e (excretion into bile) were estimated from the data. Renal intrinsic clearance ($CL_{K,int}$) was calculated from individual renal clearance values (CL_K)

$$CL_{K,\text{int}} = \frac{CL_K Q_K}{Q_K - CL_K} \quad (3)$$

where we used the CL_K values determined as cumulative urinary drug excretion divided by the serum $AUC_{0-\infty}$

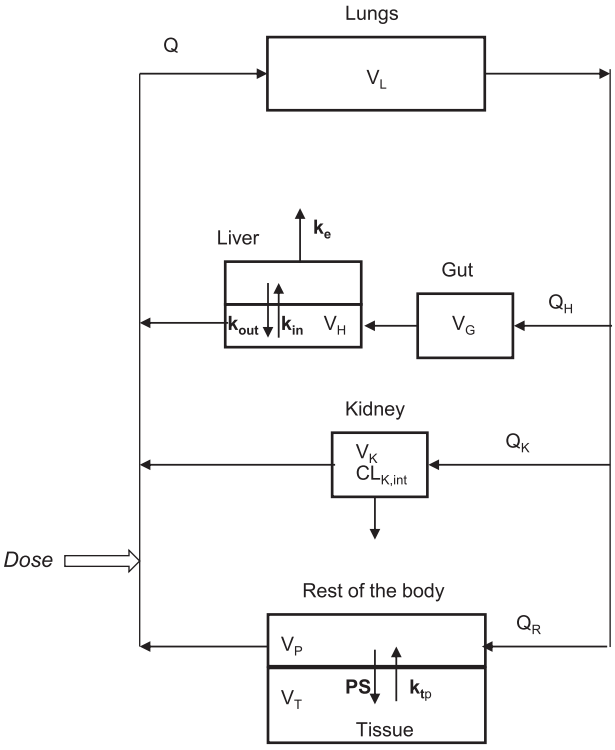

Figure 1. Structure of the minimal PBPK model of gadoxetate disposition kinetics. Bold letters denote adjustable parameters estimated by population analysis.

in reference 5; those were 74.1 ± 37.8 mL/min for the wild-type group and 76.6 ± 22.5 mL/min for the OATP1B1*1a/*1a group.

Thus, the PBPK model has 5 adjustable parameters (k_{out}, k_{in}, k_e, PS, and k_{tp}) compared with the 6 parameters of the 3-compartment model. To facilitate identifiability, we incorporated a priori information for all other parameters: systemic plasma volume (rest of the body), $V_P = 17.7$ mL/kg[15]; lung plasma volume, $V_L = 1.1V_P$; gut plasma volume, $V_G = 0.34V_P$; hepatic extracellular volume, $V_H = 0.28V_P$[16]; kidney plasma volume, $V_K = 0.05V_P$; cardiac plasma output, $Q = 2300\ (BW/70)^{0.71}$ [17]; hepatic plasma flow, $Q_H = 0.23Q$; and renal plasma flow, $Q_K = 0.2Q$.

Hepatic clearance is obtained from the estimated parameters as calculated from the liver model (see also Sirianni and Pang)[18]:

$$CL_H = \frac{Q_H k_{in} k_e}{(Q_H/V_L)(k_e + k_{out}) + k_{in}k_e} \quad (4)$$

Total clearance is given by $CL = CL_K + CL_H$.

Steady-state distribution volume is defined as the sum of all distribution volumes (Figure 1):

$$V_{ss} = 2.1\ V_P + V_T + V_H(k_{in}/k_{out}) \quad (5)$$

where the first term is the plasma volume, whereas the second and last terms account for distribution into tissues ($V_T = PS/k_{tp}$) and hepatocytes, respectively.

Results

Mammillary Compartment Model

The results of the population analysis of the gadoxetate disposition data in healthy human carriers of OATP1B1*1a/*1a and OATP1B1*15/*15 are given in Table 1 (mean model parameters and interindividual variability [CV]). The model fitted the gadoxetate disposition data well, as confirmed by the plot of the population prediction (Figure 2) and the goodness-of-fit plots (Supplementary Materials, Figure S1). Plots for the OATP1B1*15/*15 group are provided in the Supplementary Materials (Figure S2).

Physiologically Based Pharmacokinetic Model

The minimal PBPK model (Figure 1) adequately described the observed plasma concentration-time data in both study groups, and the fits were comparable to those achieved with the 3-compartment model (see Supplementary Materials, Figures S3 and S4).). For the subjects of the wild-type and OATP1B1*1a/*1a groups, the AIC values were 3271 for the PBPK model and 3305 for the 3-compartment model.

Discussion

Mammillary Compartment Model

The clearance estimate of 164.8 mL/min in carriers of the OATP1B1*1a/*1a haplotype (wild type) was in accordance with previous data[19,20]; the V_{ss} estimate of 24.1 L was larger than the extracellular fluid volume (ECV) of about 20 L in healthy human subjects. Interestingly, the distribution clearance (CL_D) of gadoxetate in our healthy carriers of the variant OATP1B1*15/*15 was significantly smaller than in carriers of the wild-type protein, OATP1B1*1a/*1a (19.2 versus 38.5 mL/min; $P < .01$). Both clearance values, however, were much smaller than those observed for the extracellular marker substance sorbitol ($CL_D = 1109$ mL/min)[21] and drugs that only distribute into the extracellular extravascular space like rocuronium ($CL_D = 861$ mL/min).[13] To illustrate the unusually slow distribution of gadoxetate in the body, Figure 3 shows the distribution curve simulated with the mean parameter values and $CL = 0$, where, asymptotically, the steady-state concentration, $C_{D,ss} = D_{iv}/V_{ss}$, is reached. From $C_{D,ss} = 48.4$ ng/mL and the mean dose, $V_{ss} = 25$ L can be derived, which is in agreement with the estimated value of 24.1 L (Table 1). For comparison, the curve simulated for rocuronium[13] is also shown in the inset. It is obvious that gadoxetate shows a

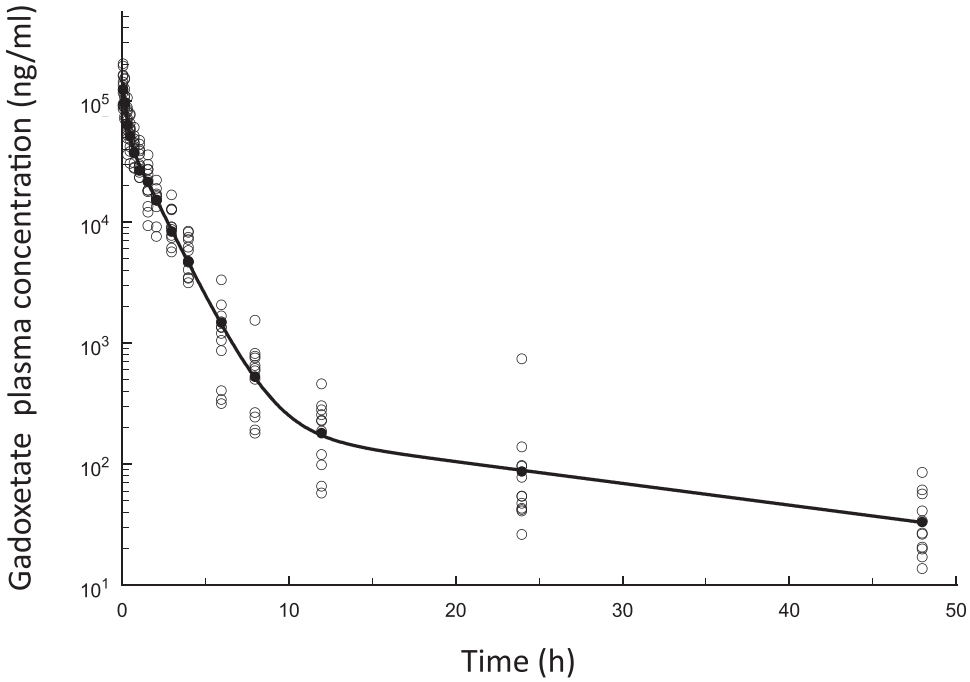

Figure 2. Fit of the gadoxetate disposition data in carriers of the wild-type OATP1B1*1a/*1a protein obtained with the 3-compartment model; with predicted population mean curve, open circles representing the observed data and filled circles their mean values.

Table 1. Parameter Estimates for the 3-Compartment Model Obtained by Population Analysis of Intravenous Gadoxetate Disposition (0.025 mmol/kg) in Humans

		*1a/*1a (n = 12)		*15/*15 (n = 9)	
Model Parameter	Symbol (Unit)	Mean	Inter-CV (%)	Mean	Inter-CV (%)
Clearance	CL (mL/min)	165	18	153	27
Volume of central compartment	V_0 (L)	6.8	19	7.32	31
Intercompartmental clearance 1	CL_{01} (mL/min)	7.73	53	4.83	40
Volume of peripheral compartment 1	V_1 (L)	10.7	37	12.5	30
Intercompartmental clearance 2	CL_{02} (mL/min)	235	35	181	23
Volume of peripheral compartment 2	V_2 (L)	6.68	27	5.15	30
Steady-state distribution volume	V_{ss} (L)	24.1	15	25.0	27
Distribution clearance	CL_M (mL/min)	38.5	64	19.2[b]	50
Residual variability[a]	s_0	11.4		1.73	
	s_1	0.249		0.267	

[a] Measurement error has a variance: $VAR_i = (\sigma_0 + \sigma_1 C[t_i])^2$.
[b] $P < .01$, exact Wilcoxon rank sum test.

much slower distribution kinetics than rocuronium: the larger area (AUC_D) between the curve and $C_{D,ss}$ reflects the lower value of CL_D (equation 2). Because CL_D is simply based on AUC_D, it does not provide information on distribution spaces involved. Thus, a PBPK model was used to get deeper insight into the underlying distribution processes.

Physiologically Based Pharmacokinetic Model

The total clearance obtained as a sum of hepatic clearance (CL_H) and renal clearance (CL_K) was in reasonable agreement (Table 2), with the value estimated with the 3-compartment model (Table 1). Furthermore, the hepatic extraction ratio, E_H, for gadoxetate of 16% was comparable with the literature values of 21%[22] and 19%[23] that were estimated with an input-output liver model using gadoxetate-enhanced MRI data. These results confirmed the usefulness of the liver model (equation 4) and our estimated parameters. Furthermore, the V_{ss} of 26.5 L was not statistically different from that estimated with the compartment model (24.1 L). The model analysis revealed that distribution into hepatocytes contributed 54% to V_{ss} (equation 5, Table 2) and that the remaining distribution volume of

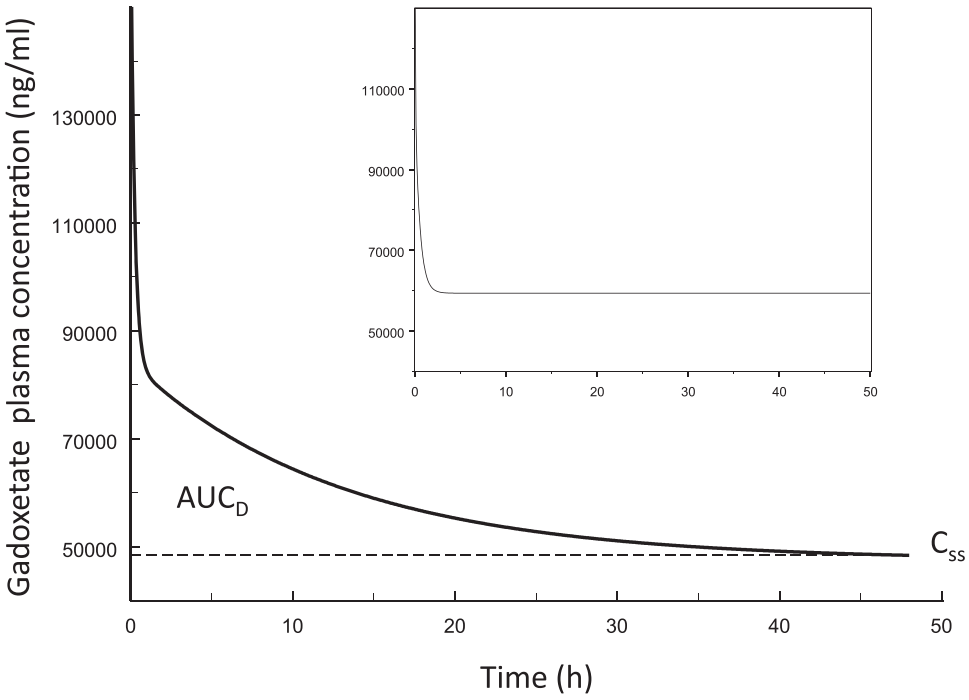

Figure 3. Distribution curve in a hypothetical noneliminating system, simulated from the population mean parameter estimates of OATP1B1*1a/*1a subjects obtained with the 3-compartment model (Table 1) assuming CL = 0. AUC_D denotes the area between the curve and the steady-state concentration $C_{ss} = C_D\ (\infty) = D_{iv}/V_{ss}$ in a hypothetical noneliminating system. For comparison, the curve simulated for rocuronium[13] is shown in the inset.

Table 2. Parameter estimates for the PBPK model (Figure 1) obtained by population analysis of intravenous gadoxetate disposition (0.025 mmol/kg) in humans

		*1a/*1a (n = 12)		*15/*15 (n = 9)	
Model parameter	Symbol (Unit)	Mean	inter CV (%)	Mean	inter CV (%)
Tissue-plasma transport rate	$k_{pt}(min^{-1})$	0.0008	32	0.0005[c]	27
Permeability-surface area product	PS (mL/min)	6.92	61	4.12[b]	47
Sinusoidal uptake rate	k_{in} (min^{-1})	6.91	40	6.65	30
Sinusoidal efflux rate	k_{out} (min^{-1})	0.15	22	0.18[c]	23
Biliary excretion rate	k_e (min^{-1})	0.0070	26	0.0075	31
Hepatic Clearance	CL_H (mL/min)	83.3	33	67.9	25
Hepatic extraction ratio	E_H (%)	16.0	38	13.0	22
Total Clearance	CL(mL/min)	159	18	147	21
Tissue distribution volume	V_T (L)	10.2	47	8.56	23
Hepatocyte distribution volume	V_{hep} (L)	14.4	28	11.3	22
Steady-state distribution volume	V_{ss} (L)	26.5	25	21.6	20
Residual variability[a]	s_0	0.1		0.1	
	s_1	0.298		0.235	

[a] Measurement error has a variance: $VAR_i = [\sigma_0 + \sigma_1 C(t_i)]^2$
[b] $P<0.05$, Exact Wilcoxon rank-sum test
[c] $P<0.01$, Exact Wilcoxon rank-sum test

~12 L was smaller than the ECV of ~20 L. This means that the V_{ss} estimate of about 20 L observed in previous studies[6,7] may have misleadingly led to the conclusion that gadoxetate distributes rapidly throughout the ECV.

An instructive explanation of the whole-body distribution kinetics of gadoxetate is given in Figure 4. The simulated amount-time courses in plasma, tissue, and hepatocytes confirmed the fast uptake of gadoxetate

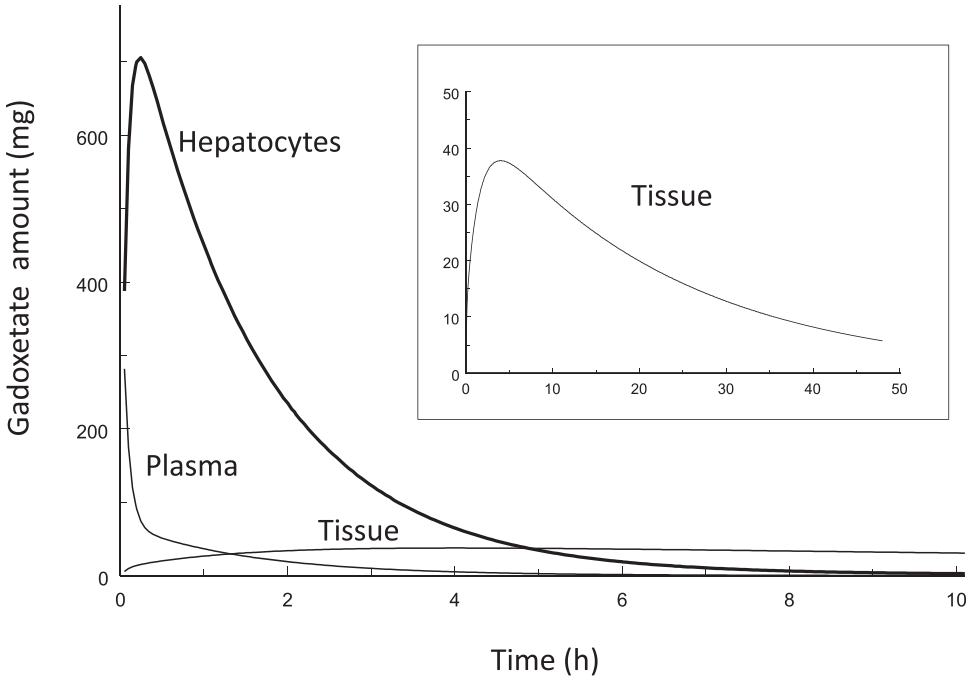

Figure 4. Time amount-time courses of gadoxetate in plasma, hepatocytes, and nonhepatic tissues (Tissue) as predicted by the PBPK model (Figure 1). The inset shows the amount in tissues in a different scale. The curves were simulated from the population mean parameter estimates for healthy subjects with OATP1B1*1a/*1a subjects (Table 2).

into hepatocytes in less than 30 minutes. The hepatocyte curve peaks at about 20 minutes, which is in good agreement with the peak enhancement in gadoxetate-enhanced liver MRI.[3,5] Furthermore, the peak amount of 700 mg is consistent with the estimates obtained by modeling of enhancement kinetics.[23] In interpreting that the simulated curve declines somewhat faster than liver parenchymal enhancement,[5] one should take into account that the latter may not be proportional to concentration.

Into other tissues, gadoxetate distributes extremely slowly, with a maximum after approximately 5-6 hours. The nature of this tissue distribution process characterized by an extremely low value of PS (compared with extracellular markers) remains unclear. The rapid initial decline of the plasma concentration-time curve after intravenous bolus injection is most likely caused by extensive uptake of gadoxetate into the liver rather than by distribution into the extracellular extravascular space. Up to now, it has been known that gadoxetate distributes in humans into kidney, neuronal, and other tissues.[24]

The low distribution clearance of gadoxetate can be explained by 2 factors: (1) hepatic uptake occurs at a lower rate than extravasation of extracellular markers and (2) distribution in tissues outside the liver is delayed and very slow (slow terminal equilibration). The estimate of the permeability-surface area product (PS = 6.92 mL/min) of gadoxetate is nearly 2 orders of magnitude lower than that estimated for inulin (330 mL/min),[25] insulin (75 mL/min),[14] and rocuronium (614 mL/min)[12] despite quite similar molecular weights of the drugs. Note also that our value of PS = 6.92 mL/min is in line with that estimated with a somewhat different model used by Forsgren et al.[19] However, hepatic uptake seems to be the major determinant of the distribution clearance, CL_D, as shown in Figure 5, which displays the dependence on the k_{in}/k_{out} ratio ($r = 0.77$, $P < .0001$).

Our results are in good agreement with the hepatic-pharmacokinetic conception on gadoxetate-enhanced liver MRI that accumulation of contrast agent results is the net result of the interplay of, first, extremely rapid hepatic uptake ($k_{in} = 6.91$/min) via OATP1B1, OATP1B3, and sodium/taurocholate cotransporting polypeptide, as driven by the high serum concentrations immediately after bolus injection with, second, an about 50 times slower sinusoidal efflux ($k_{out} = 0.146$/min) via MRP3 and, third, extremely slow biliary excretion ($k_e = 0.07$/min) via MRP2 (Table 2).[4,26] The uptake into nonhepatic tissues can be caused most likely by OATP1A2, to which gadoxetate has high affinity[4] and which has been located in the apical membrane of brain capillary endothelial cells and renal tubular cells. The uptake rate by OATP1A2, however, might be rather small because both membrane sites are equipped with secretory MRPs counteracting the porous uptake of gadoxetate.[27]

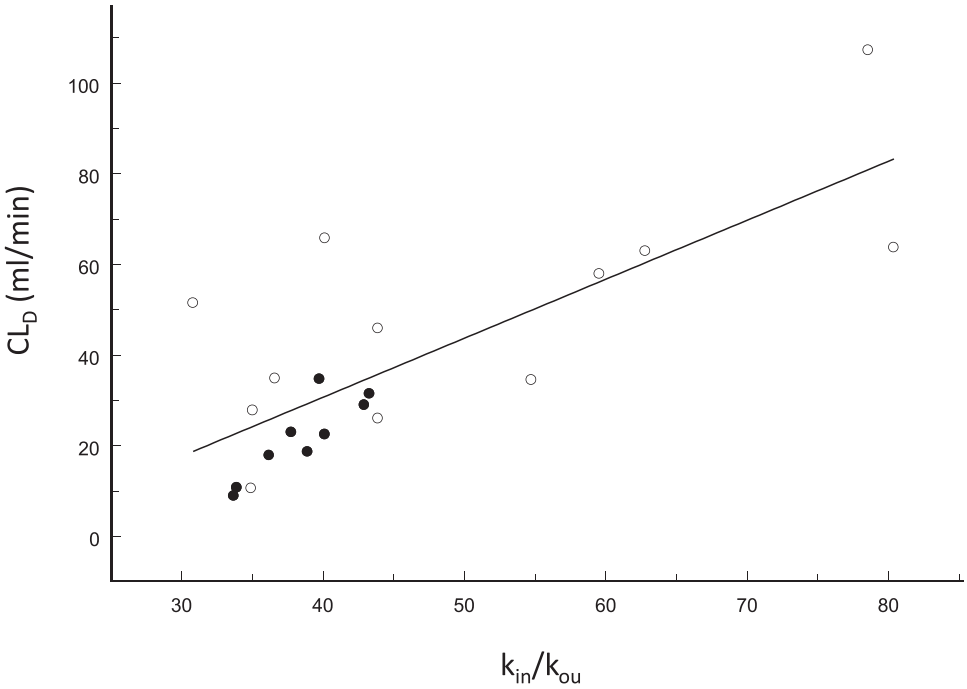

Figure 5. Distribution clearance CL_D of gadoxetate estimated with the 3-compartment model increases with the ratio of hepatic uptake to efflux constant estimated with the PBPK model ($r = 0.77, P < .0001$). Filled circles represent carriers of OATP1B1*15/*15 and empty circles the wild-type OATP1B1 *1a/*1a subjects.

Based on the liver parenchymal enhancement by gadoxetate and in vitro transport results, we have supposed that the uptake of the contrast agent is lowered in subjects with OATP1B1*15/*15, a genetic loss-of-function protein variant of the transporter.[5,28] Our reevaluation of the serum concentration-time data by the minimal PBPK model, however, could not confirm that the sinusoidal uptake-rate is reduced. Instead, we unexpectedly found the sinusoidal efflux rate significantly increased in subjects with the variant *15/*15 protein compared with the wild type, *1a/*1a (0.146/min vs 0.175/min; $P < .001$). The apparent hepatic distribution volume decreases from 14.4 to 11.3 L, whereas the biliary excretion rate remained unchanged. Note that the observed apparent (nonsignificant) decrease in CL_H and E_H in subjects with *15/*15 is in line with the higher sinusoidal efflux rate. Obviously, according to our modeling, gadoxetate seems to be extracted from the sinusoidal blood still with an unrestricted rate by the deficient OATP1B1 transporter protein. The mechanisms behind the upregulated sinusoidal efflux (back) secretion (increase in k_{out}), most likely via the active ATP-driven MRP3, is not yet clear. However, expression of hepatic drug transporters can be modified in experimental liver diseases (fibrosis, cirrhosis), whereby decrease of OATP and MRP2 and an increase of MRP3 expression were observed.[29] In rats with advanced fibrosis, hepatic uptake and biliary secretion decreased and the sinusoidal back-flux increased, significantly correlated WITHthe expression of OATP1A1, MRP2, and MRP3, respectively.[30]

Another unexpected finding of the PBPK modeling was that healthy carriers of the variant OATP1B1*15/*15 transporter showed both slower tissue uptake (PS = 4.12 vs 6.92 mL/min, $P < .05$) and reduced tissue-to-plasma transport constant, k_{tp} (0.0005/min vs 0.0008/min, $P < .05$) compared with carriers of OATP1B1*1a/*1a. This finding together with the lower k_{in}/k_{out} ratio (38.5 vs 50.1; compare with Figure 5) explains the slower distributional equilibration process observed in these subjects (50% lower CL_D). The significant correlation between CL_D and k_{tp} ($r = 0.66$, $P < .001$) is depicted in Figure 6; the correlation between CL_D and PS was less expressed ($r = 0.48$) but also significant ($P < .05$).

With respect to a potential role of active drug transporters rather than passive nonionic diffusion into the nature of tissue distribution and the low value of PS (compared with extracellular markers), the nearly complete correlation between PS and k_{tp} in the subjects with the deficient OATP1B1*15/*15 is striking ($r = 0.99$, $P < .0001$; Supplementary Materials, Figure S5). The correlation was less pronounced in the wild-type OATP1B1*1a/*1a group. Obviously, the putative uptake and efflux transporters are coordinately downregulated in these subjects. However, the molecular mechanisms behind the need to be evaluated in future studies.

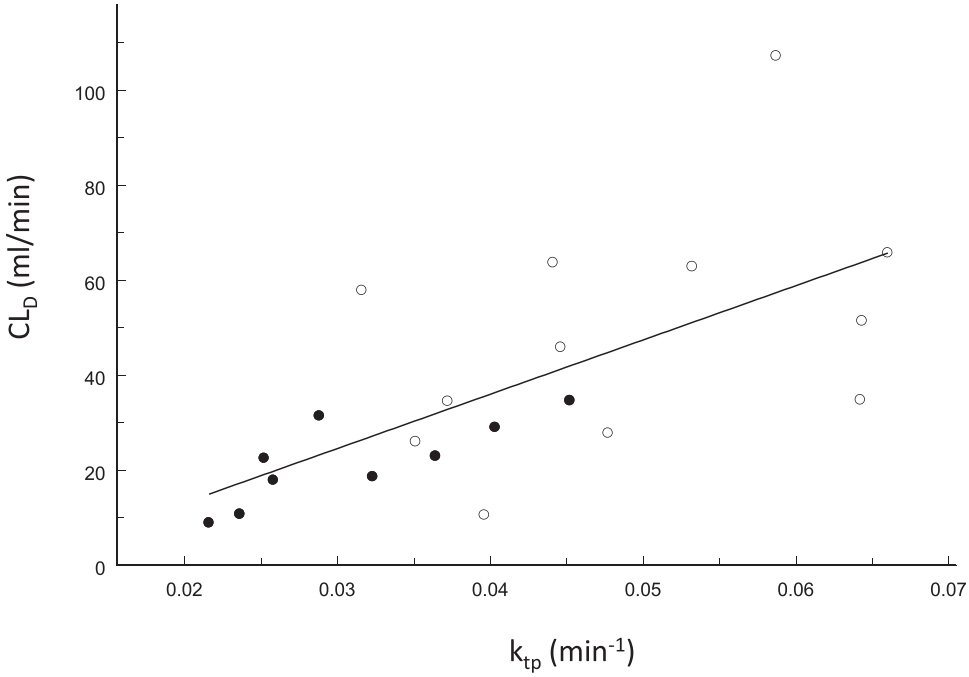

Figure 6. Distribution clearance CL_D of gadoxetate increases with tissue-to-plasma transport constant k_{tp} estimated with the PBPK model ($r = 0.66$, $P < .001$). Filled circles represent carriers of OATP1B1*15/*15 and empty circles the wild-type OATP1B1 *1a/*1a subjects.

In interpreting the results of the pharmacokinetic analysis, the following limitations should be considered. Although the result on distribution kinetics of gadoxetate (low distribution clearance) is independent of a specific pharmacokinetic model, one should keep in mind that those obtained with the minimal PBPK model are model dependent, making them valid only under the specific assumptions and in relation to the underlying data. Although the goodness of fit and the reliability of parameter estimates (indicated by the reasonably low CVs and correlation coefficients) support the validity of the model, this is only a necessary but not sufficient condition. More importantly, both the time course of the amount of gadoxetate in hepatocytes as predicted by the model (Figure 4) and the hepatic extraction ratio were in accordance with results obtained with dynamic gadoxetate-enhanced MR imaging.[5,24]

Although compared with direct uptake measurements with gadoxetate-enhanced MRI, an analysis on the basis of plasma concentration-time data may not be suitable to detect small changes in hepatocellular uptake, our results are not in contradiction with previous ones in the literature. In other words, as long as the answers given by our model cannot be disproved, they may induce a reconsideration of present interpretations.

Conclusions

The rapid initial distribution phase is not brought about by distribution of gadoxetate into the extracellular extravascular space, but by fast uptake into the hepatocytes. Healthy carriers of the variant OATP1B1*15/*15 transport protein have a higher sinusoidal efflux rate than those of the wild-type OATP1B1*1a/*1a protein. The distribution into tissue (outside the liver) is rather slow, with peak uptake about 5 hours after intravenous administration; the permeability-surface area product and the tissue-to-plasma distribution rate are reduced in the OATP1B1*15/*15 group. However, the interplay of the transporters suggested by the model is open to future debate; further work is necessary to clarify the role of hepatocyte influx and efflux in determining hepatic uptake and whole-body distribution kinetics.

Acknowledgment

Open access funding enabled and organized by Projekt DEAL.

Conflicts of Interest

The authors declare no conflicts of interest.

Data Sharing

All data that were evaluated in our article are filed by the University Medicine of Greifswald and can be obtained by contacting Dr. Werner Siegmund (werner.siegmund@uni-greifswald.de).

References

1. Weiss M, Ring A. Interpretation of general measures of distribution kinetics in terms of a mammillary compartmental model. *J Pharm Sci*. 1997;86(12):1491-1493.
2. Weiss M. Residence time dispersion as a general measure of drug distribution kinetics: estimation and physiological interpretation. *Pharm Res*. 2007;24(11):2025-2030.
3. Van Beers BE, Pastor CM, Hussain HK. Primovist, Eovist: what to expect? *J Hepatol*. 2012;57(2):421-429.
4. Jia J, Puls D, Oswald S, et al. Characterization of the intestinal and hepatic uptake/efflux transport of the magnetic resonance imaging contrast agent gadolinium-ethoxylbenzyl-diethylenet riamine-pentaacetic acid. *Invest Radiol*. 2014;49(2):78-86.
5. Nassif A, Jia J, Keiser M, et al. Visualization of hepatic uptake transporter function in healthy subjects by using gadoxetic acid-enhanced MR imaging. *Radiology*. 2012;264(3):741-750.
6. Aime S, Caravan P. Biodistribution of gadolinium-based contrast agents, including gadolinium deposition. *J Magn Reson Imaging*. 2009;30(6):1259-1267.
7. Gschwend S, Ebert W, Schultze-Mosgau M, Breuer J. Pharmacokinetics and imaging properties of Gd-EOB-DTPA in patients with hepatic and renal impairment. *Invest Radiol*. 2011;46(9):556-566.
8. Yamada A, Hara T, Li F, et al. Quantitative evaluation of liver function with use of gadoxetate disodium-enhanced MR imaging. *Radiology*. 2011;260(3):727-733.
9. Kang Y, Lee JM, Kim SH, Han JK, Choi BI. Intrahepatic mass-forming cholangiocarcinoma: enhancement patterns on gadoxetic acid-enhanced MR images. *Radiology*. 2012;264(3):751-760.
10. Quaia E, Angileri R, Arban F, Gennari AG, Cova MA. Predictors of intrahepatic cholangiocarcinoma in cirrhotic patients scanned by gadobenate dimeglumine-enhanced magnetic resonance imaging: diagnostic accuracy and confidence. *Clin Imaging*. 2015;39(6):1032-1038.
11. D'Argenio DZ, Schumitzky, Wang, F. *ADAPT 5 user's Guide: Pharmacokinetic/Pharmacodynamic Systems Analysis Software*. Los Angeles, CA: Biomedical Simulations Resource; 2009.
12. Weiss M, Pang KS. Dynamics of drug distribution. I. Role of the second and third curve moments. *J Pharmacokinet Biopharm*. 1992;20(3):253-278.
13. Weiss M. Comparison of distributed and compartmental models of drug disposition: assessment of tissue uptake kinetics. *J Pharmacokinet Pharmacodyn*. 2016;43(5):505-512.
14. Weiss M, Tura A, Kautzky-Willer A, Pacini G, D'Argenio DZ. Human insulin dynamics in women: a physiologically based model. *Am J Physiol Regul Integr Comp Physiol*. 2016;310(3):R268-R274.
15. Weiss M, Reekers M, Vuyk J, Boer F. Circulatory model of vascular and interstitial distribution kinetics of rocuronium: a population analysis in patients. *J Pharmacokinet Pharmacodyn*. 2011;38(2):165-178.
16. Nilsson H, Blomqvist L, Douglas L, et al. Gd-EOB-DTPA-enhanced MRI for the assessment of liver function and volume in liver cirrhosis. *Br J Radiol*. 2013;86(1026):20120653.
17. Collis T, Devereux RB, Roman MJ, et al. Relations of stroke volume and cardiac output to body composition: the strong heart study. *Circulation*. 2001;103(6):820-825.
18. Sirianni GL, Pang KS. Organ clearance concepts: new perspectives on old principles. *J Pharmacokinet Biopharm*. 1997;25(4):449-470.
19. Forsgren MF, Dahlqvist Leinhard O, Dahlstrom N, Cedersund G, Lundberg P. Physiologically realistic and validated mathematical liver model reveals [corrected] hepatobiliary transfer rates for Gd-EOB-DTPA using human DCE-MRI data. *PLoS One*. 2014;9(4):e95700.
20. Schuhmann-Giampieri G, Mahler M, Roll G, Maibauer R, Schmitz S. Pharmacokinetics of the liver-specific contrast agent Gd-EOB-DTPA in relation to contrast-enhanced liver imaging in humans. *J Clin Pharmacol*. 1997;37(7):587-596.
21. Weiss M, Hubner GH, Hubner IG, Teichmann W. Effects of cardiac output on disposition kinetics of sorbitol: recirculatory modelling. *Br J Clin Pharmacol*. 1996;41(4):261-268.
22. Nilsson H, Nordell A, Vargas R, Douglas L, Jonas E, Blomqvist L. Assessment of hepatic extraction fraction and input relative blood flow using dynamic hepatocyte-specific contrast-enhanced MRI. *J Magn Reson Imaging*. 2009;29(6):1323-1331.
23. Georgiou L, Penny J, Nicholls G, et al. Quantitative assessment of liver function using gadoxetate-enhanced magnetic resonance imaging: monitoring transporter-mediated processes in healthy volunteers. *Invest Radiol*. 2017;52(2):111-119.
24. McDonald RJ, McDonald JS, Kallmes DF, et al. Intracranial gadolinium deposition after contrast-enhanced MR imaging. *Radiology*. 2015;275(3):772-782.
25. Keiding S, Henriksen O, Sejrsen P. Muscle capillary permeability for [14C]inulin and [51Cr]EDTA in human forearm. *Acta Physiol Scand*. 1988;133(3):335-342.
26. Leonhardt M, Keiser M, Oswald S, et al. Hepatic uptake of the magnetic resonance imaging contrast agent Gd-EOB-DTPA: role of human organic anion transporters. *Drug Metab Dispos*. 2010;38(7):1024-1028.
27. Ivanyuk A, Livio F, Biollaz J, Buclin T. Renal drug transporters and drug interactions. *Clin Pharmacokinet*. 2017;56(8):825-892.
28. Yee SW, Brackman DJ, Ennis EA, et al. Influence of transporter polymorphisms on drug disposition and response: a perspective from the international transporter consortium. *Clin Pharmacol Ther*. 2018;104(5):803-817.
29. Gu X, Manautou JE. Regulation of hepatic ABCC transporters by xenobiotics and in disease states. *Drug Metab Rev*. 2010;42(3):482-538.
30. Giraudeau C, Leporq B, Doblas S, et al. Gadoxetate-enhanced MR imaging and compartmental modelling to assess hepatocyte bidirectional transport function in rats with advanced liver fibrosis. *Eur Radiol*. 2017;27(5):1804-1811.

Supplemental Information

Additional supplemental information can be found by clicking the Supplements link in the PDF toolbar or the Supplemental Information section at the end of web-based version of this article.